



Production of drop-in biodiesel blendstocks via competitive acid-catalyzed dehydration reactions using ethanol oligomerization products

Journal:	<i>Sustainable Energy & Fuels</i>
Manuscript ID	SE-ART-03-2024-000362.R1
Article Type:	Paper
Date Submitted by the Author:	13-Apr-2024
Complete List of Authors:	Canales, Emmanuel ; University of Wisconsin-Madison Hower, Samuel; University of Wisconsin, Chemical and Biological Engineering Li, Daniel; University of Wisconsin, Chemical and Biological Engineering Tambe, Aditya; University of Wisconsin, Chemical and Biological Engineering Rothamer, David; University of Wisconsin-Madison, Mechanical Engineering Huber, George; University of Wisconsin, Chemical and Biological Engineering

Production of drop-in biodiesel blendstocks via competitive acid-catalyzed dehydration reactions using ethanol oligomerization products

**Authors: Emmanuel Canales^a, Samuel C. Hower^a, Daniel Paul Li^a,
Aditya Tambe^a, David Rothamer^b, George W. Huber^a**

^a*Department of Chemical and Biological Engineering, University of Wisconsin–Madison, USA. E-mail: gwhuber@wisc.edu.*

^b*Department of Mechanical Engineering, University of Wisconsin–Madison, USA*

Abstract

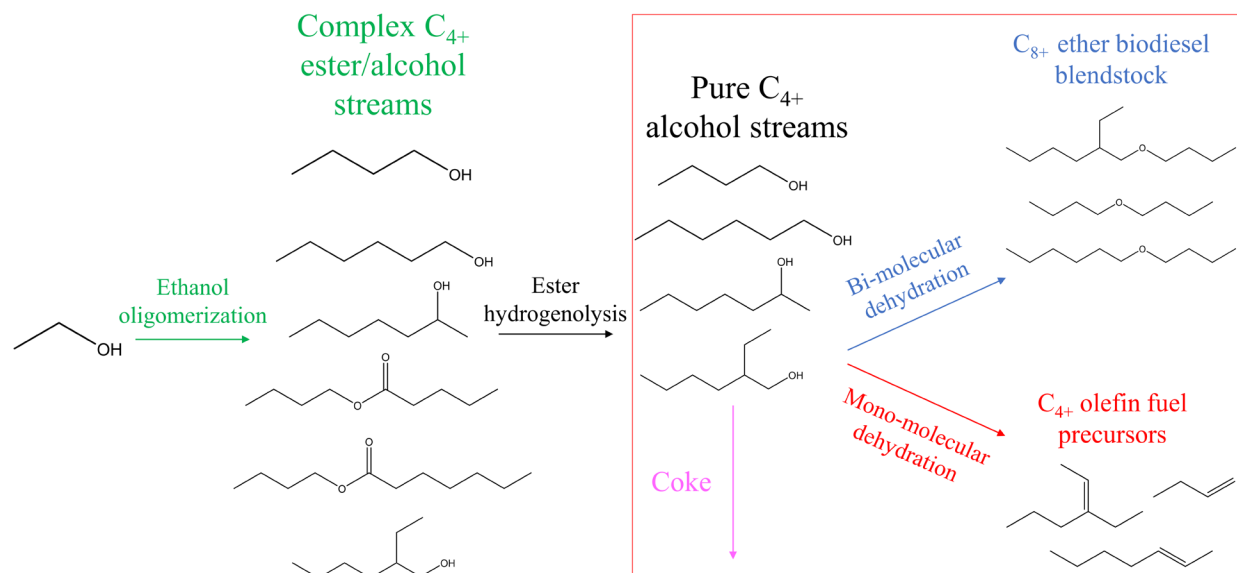
Ethanol can be converted into diesel fuel ethers using a three-step catalytic approach that involves ethanol oligomerization to larger alcohols, hydrogenolysis of the esters followed by dehydration of the C₄ to C₈ alcohols into ethers. In this paper we report results for the dehydration of a mixture of C₄ – C₈ alcohols using a zeolite Y catalyst in a continuous flow reactor. Mono-molecular dehydration of the alcohols produces olefins while bi-molecular dehydration of the alcohol produces ethers. Increasing the pressure increases the ether selectivity while decreasing the pressure produces more olefins. Linear alcohol feeds produce more C₈₊ ethers, while branched and secondary alcohols lead to more olefins. Olefin and coke selectivities increase with increasing carbon chain length of alcohols. Secondary alcohols lead to higher coke selectivities. Ethanol/Butanol oligomerization experiments showed that the incoming dehydration feedstock can be grown to larger C₆₊ alcohol fractions, leading to higher yields of C₁₀₊ diesel-range ethers.

1 Introduction

There is a clear societal need to produce low-carbon liquid transportation fuels. In this respect biomass is an inexpensive renewable carbon source that is being used today to produce liquid transportation fuels. The most widely used biofuel is ethanol^{3,4}. Ethanol is used as a gasoline blendstock^{3,4}. In the US, around 10 vol% of ethanol is blended into gasoline⁵. As more electric vehicles are used for light duty transportation vehicles, the demand for gasoline, and also the demand for ethanol, is decreasing. However, the demand for heavy transportation fuel is projected to increase⁶. Electrification of transportation for heavy duty vehicles is difficult due to the low energy density, slow charging time, and high cost of batteries^{7,8}. New approaches for upgrading ethanol to heavier distillate-range fuels (sustainable aviation fuels and diesel fuels) are needed. A number of approaches have focused on ethanol conversion into jet fuel and these technologies are moving towards commercialization³. These approaches primarily focus on jet fuel by producing heavily branched alkanes. However, the branching of alkanes leads to a low cetane number^{3,9}, and only a fraction of these alkanes are in the diesel fuel range⁹.

We have previously proposed a three-step process to convert ethanol into distillate-range ethers as outlined in Scheme 1². The process first involves ethanol oligomerization to C₄₊ oxygenates which is rich in alcohols over a Cu/Mg_xAl_yO catalyst¹⁰. This process creates a distribution of oxygenate molecules consisting of C₄₊ alcohols, aldehydes, ketones, and esters. The second step is an ester hydrogenolysis step that hydrogenates esters in this oxygenate stream into alcohols. The products from the hydrogenolysis reactor are a mixture of C₄₊ linear, branched, and secondary alcohols. The last step is dehydration which produces C₈₊ ethers and C₄₊ olefins. Mono-molecular dehydration produces olefins while bimolecular dehydration produces ethers. These ethers possess higher cetane number than diesel fuel. The ethers also have the appropriate boiling point and low volatility suggesting they can be used in diesel blends¹¹. C₁₀₊ ethers also have lower sooting index, water solubility and higher flashpoint temperatures compared to lower

chain ethers¹². Ethers produced from C₆₊ alcohol streams have similar properties relative to diesel #2. While butyl ether may be used as a diesel additive, blending limits can be influenced based on the minimum flashpoint requirement for a diesel #2 blend (> 52 °C), as shown in Figure SI1.



Scheme 1. Three step process chemistry for ethanol to diesel-range ethers.

The objective of this paper is to study the catalytic dehydration of mixtures of ethanol oligomerization products over a zeolite Y catalyst in a continuous flow reactor. We try to understand how the reaction conditions and different feed components influence the product selectivity, catalytic activity, and catalytic deactivation for dehydration reactions. Over 100 different products are produced during ethanol oligomerization including linear, branched and secondary C₄₋₁₀ alcohols, aldehydes, ketones, and esters with the primary products being linear alcohols¹⁰. Figure 1^{1, 2} shows the simulated Guerbet (SG) feedstocks that we will use for etherification in this publication. The SG feed assumes that all the products lighter than C₄ from ethanol oligomerization are distilled and the ketones, aldehydes and acetals are hydrogenated to their respective alcohols. The product selectivity for ethanol oligomerization is a function of conversion¹⁰. Figure 1 shows the SG product selectivity at four different ethanol conversions from ethanol oligomerization². (e.g. SG-12 represents the simulated Guerbet product from ethanol oligomerization at 12 % ethanol conversion and assuming the ketones, aldehydes and acetals are hydrogenated to their respective alcohols).

The final SG mixtures are a distribution of linear alcohols, branched alcohols, secondary alcohols, and esters. The left-hand side of the graph represents the mol fractions of linear alcohols, while the right-hand axis represents the mol fractions of secondary and branched alcohols, in addition to esters. At an ethanol conversion of 12%, n-butanol is the main product, with low amounts of C₆₊ alcohols and esters. As the ethanol conversion increases, the size of the alcohols produced increases. The secondary and branched alcohol content and the ester content increase with increasing conversion as well.

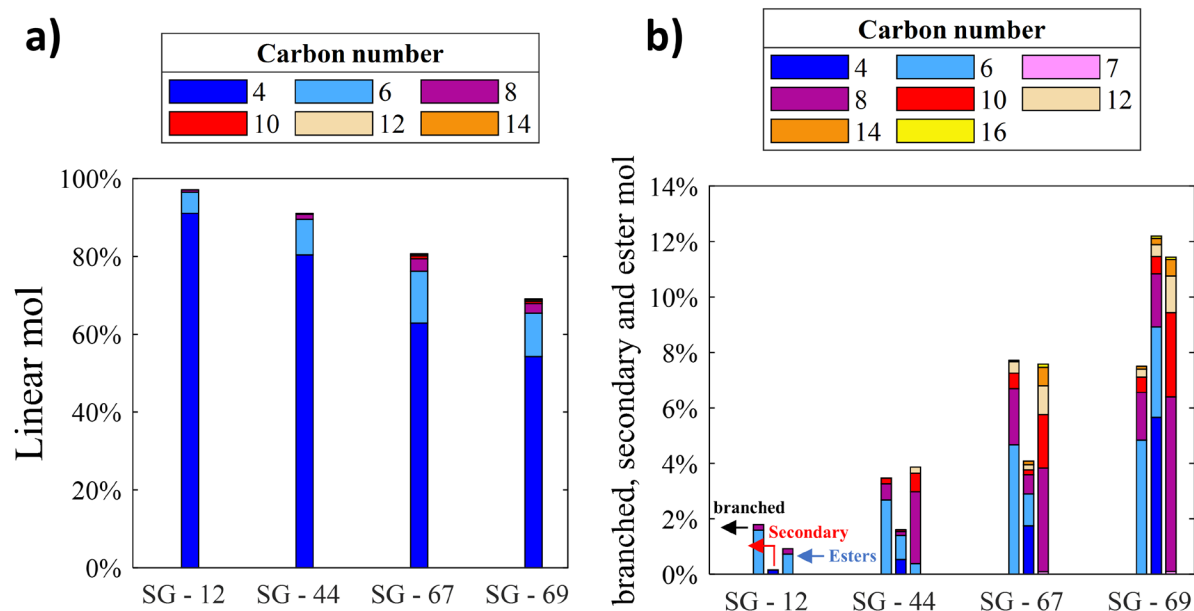


Figure 1. Oxygenate distribution of products from ethanol oligomerization as a function of ethanol conversion. These products will be used as feeds for the etherification experiments in this paper. The conversion was varied by changing the weight hourly space velocity in the reactor. The conversion is shown after the dash. **A)** represents the linear alcohol distribution and **B)** represents the branched and secondary alcohol distributions, as well as the ester distributions. For secondary alcohols, the numbering is defined by ‘n+1’. Colors not visibly shown for compounds are present in low amounts (< 1.0%). Data taken from^{1,2}.

In this study, we demonstrate how dehydration of ethanol oligomerization products produces distillate range ethers with selectivities ranging from 60% to 80% in a continuous flow reactor with Zeolite HY. We also demonstrate the ability to tune reactant feedstock distributions, which allows for tuning the final average carbon number of the fuel mixtures produced. The oxygenate products are feedstocks that have varying size distributions depending on the ethanol conversion in the first step (10% to 69%), as shown in Figure 1. A more detailed breakdown of feedstock compositions used in this paper can be seen in the SI (See Tables SII – 4 in SI section 1). For more information on the detailed composition of the final dehydration products, refer to Tables SI5 – SI14 in SI section 2.

2 Experimental

2.1 Reactor design and specifications

The etherification of oxygenate species was performed in stainless-steel fixed bed reactors packed with Zeolite HY (Zeolyst International, CBV-720). The commercial catalyst has a Si/Al ratio of 30, with a surface area of 780 m²/g. The reactor was typically 33 cm long with a catalyst bed length of 17.8 cm, using an outer diameter of 0.95 cm. For bed packing, Quartz wool (Acros Organics, Coarse 9 –30 microns) and silicon dioxide (Sigma Aldrich, fused – granular, 4-20 mesh, 99.9% trace metals basis) was used. Prior to loading into the reactor, large batches of zeolite were calcined overnight at 600 °C in a muffle furnace in static air, with a ramp of 4 °C/min. The catalyst was then dried at 110 °C until use. Catalyst beds were diluted with silica chips (Sigma Aldrich) to minimize pressure drop, typically with a 1:2 g_{cat} to g_{beads} ratio. The beads were typically crushed to a size between 30 – 80 mesh (ASTM). Reactant feedstocks were fed with an HPLC pump (Eldex), typically between 0.02 – 0.04 mL/min. Ar was used as the cofeed inert gas, typically with a flowrate of 10 mL/min. The reactor was heated using a furnace (Applied Test Systems,

Series 3210) and kept uniform using aluminum blocks. The exact reactor dimensions, bed dilution ratios, gas flowrates, feed flowrates, and analytical techniques used to identify liquid and gas species can be found elsewhere².

2.2 Quantification of coke products

The total organic content (TOC) experiments on the catalyst beds were analyzed using a total organic carbon analyzer (Shimadzu, TOC – V) to establish estimated solid coke flowrates, using a carrier gas flowrate of 150 mL/min. Coke flowrates were then used to close carbon balances, with experimental error being less than or equal to 10% for all beds studied. In this paper, we therefore assume that all missing carbon is due to coke products. A more detailed explanation can be found in SI section 3 and Tables SI15 – 17. Thermogravimetric analysis (TGA) experiments on catalyst beds were conducted in a TA instruments Q500 Thermogravimetric Analyzer. The ramp was set at 20 °C/min and heated to 800 °C. For both oxygen and nitrogen experiments, a 50 mL/min flowrate was used with a balance inert gas flowrate of 50 mL/min. The TGA results can be found in Figure SI3 in SI section 3. For etherification species that overlapped, a qualitative analysis in glass batch reactors was performed to identify cross-etherification species (See Figure SI5, SI section 4). For information on the TOS conversion of each reactant for each experiment, refer to Tables SI18 – SI30 and Figures SI6 – SI13 in SI section 5.

2.3 Analytical techniques and representation of alcohol oligomerization and dehydration products

The alcohols 1-butanol (Sigma Aldrich, 99.8% anhydrous), 1-hexanol (Sigma Aldrich, >99% anhydrous), 1-octanol (Alfa Aesar, 99%), 1-decanol (Alfa Aesar, 98+%), 1-dodecanol (Thermo Scientific, 98%) and 1-tetradecanol (Acros Organics, 99%) were obtained to represent the linear alcohols obtained from the ethanol oligomerization reactor. The alcohols 2-methyl-1-butanol (Thermo Scientific, 98%), 2-ethyl-1-butanol (Sigma Aldrich, 98%) and 2-ethyl-1-hexanol (Frontier Scientific, 99%) were used to represent branched alcohols. 2-butanol (TCI chemicals, >99%), 2-pentanol (Sigma Aldrich, 98%), 2-heptanol (Acros Organics, 99+%), 2-octanol (TCI chemicals, >98%), 4-nonanol (Santa Cruz Biotechnology, >98%), 2-nonanol (Sigma Aldrich, 99%), and 2-undecanol (Alfa Aesar, 98+%) were obtained to represent secondary alcohols. The esters ethyl butanoate (Sigma Aldrich, 99%), butyl acetate (TCI chemicals, 99+%) and ethyl hexanoate (Sigma Aldrich, 99%) were obtained to represent the esters obtained from the ethanol oligomerization reactor. 1-heptanol (Acros Organics, 98%) and dodecane (Sigma Aldrich, >99% anhydrous) were used for diluting the product mixture to prepare analytical samples. 1-heptanol was used for alcohol feeds, while dodecane was used when esters were present to avoid overlapping of products. Dodecane and n-decane (Alfa Aesar, 99+%) were used as the inert solvents for qualitative analysis of cross-etherification products. For analysis of liquid samples post – reaction using gas chromatography, tetrahydrofuran (99+% Stab. with 250ppm BHT) was used to homogenize the aqueous and organic phase. Calibration standards for liquid products such as ethers and olefins were obtained from the manufacturers mentioned. For the TOC experiments, Potassium hydrogen phthalate (Acros Organics, primary standard) was used to create a four-point calibration curve for quantification of carbon uptake on the catalyst beds.

2.4 Quantification of the final products from dehydration reactions

Yields were calculated according to Equation (1) on a carbon basis, where \dot{n}_i is the flowrate of the carbon species. Because not all the GC area was assigned to known species, the yield of unknown carbon in the gas and liquid phase were estimated by Equation (2), and selectivities were also calculated on a carbon basis based on Equation (3), as shown elsewhere¹¹. Since there was overlap between product species in the GC chromatogram, overlapped area was assigned based on GC-MS area overlaps. The ratio of the areas of one product to another, defined as R_{Area} , was assumed to be constant and was then used for the GC-

FID area overlaps. The areas were then split into their respective products. Equation (4) summarizes the GC-area estimation of overlapped products. The overall carbon conversion is represented by Equation (5) and is based on the total carbon converted. The conversion for each reactant is further defined by equation (6). Equation (7) represents the carbon balance prior to analyzing for coke. In this paper, all carbon balances calculated are based on equation (7). Equation (8) is the carbon balance once coke products are analyzed. Equation (8) is used to adjust the final carbon balances for the reaction runs, which can be found in the SI. Not all runs added up to 100% carbon balance after considering coke products from the TOC experiments. This implies that there is missing mass that could not be accounted for with our analytical methods. $\dot{n}_{C, \text{ olig}}$ represents the final missing carbon that could not be accounted for. This carbon is likely in the form of heavy oligomers, which cannot be detected by our GC – methods.

$$\text{Yield}_i = \frac{\dot{n}_{C_i, \text{ out}}}{\dot{n}_{C \text{ total}, \text{ in}}} \quad (1)$$

$$\text{Yield}_{\text{unknown}} = \frac{A_{\text{unidentified products}}}{A_{\text{total products}}} * \sum_i Y_{i, \text{ products}} \quad (2)$$

$$\text{Selectivity}_i = \frac{Y_i}{X} \quad (3)$$

$$R_{\text{Area, MS}} = \frac{A_{x, \text{ MS}}}{A_{y, \text{ MS}}} = \frac{A_{\text{total, FID}} - A_{y, \text{ FID}}}{A_{y, \text{ FID}}} = \frac{A_{\text{total, FID}}}{A_{y, \text{ FID}}} - 1 \quad (4)$$

$$\text{Overall conversion (X)} = \frac{\dot{n}_{C \text{ total}, \text{ in}} - \dot{n}_{C \text{ total}, \text{ out}}}{\dot{n}_{C \text{ total}, \text{ in}}} \quad (5)$$

$$\text{Conversion}_i = \frac{\dot{n}_{C_i, \text{ in}} - \dot{n}_{C_i, \text{ out}}}{\dot{n}_{C_i, \text{ in}}} \quad (6)$$

$$\text{Carbon balance} = \frac{\dot{n}_{C, \text{ total liquid prods}} + \dot{n}_{C, \text{ total gas products}}}{\dot{n}_{C \text{ total}, \text{ in}}} \quad (7)$$

$$\text{Carbon balance}_{\text{adjusted}} = \frac{\dot{n}_{C, \text{ total liquid prods}} + \dot{n}_{C, \text{ total gas products}} + \dot{n}_{C, \text{ coke products}} + \dot{n}_{C, \text{ olig products}}}{\dot{n}_{C \text{ total}, \text{ in}}} \quad (8)$$

3 Results/discussion

3.1 Thermodynamics of bi-molecular and mono-molecular dehydration

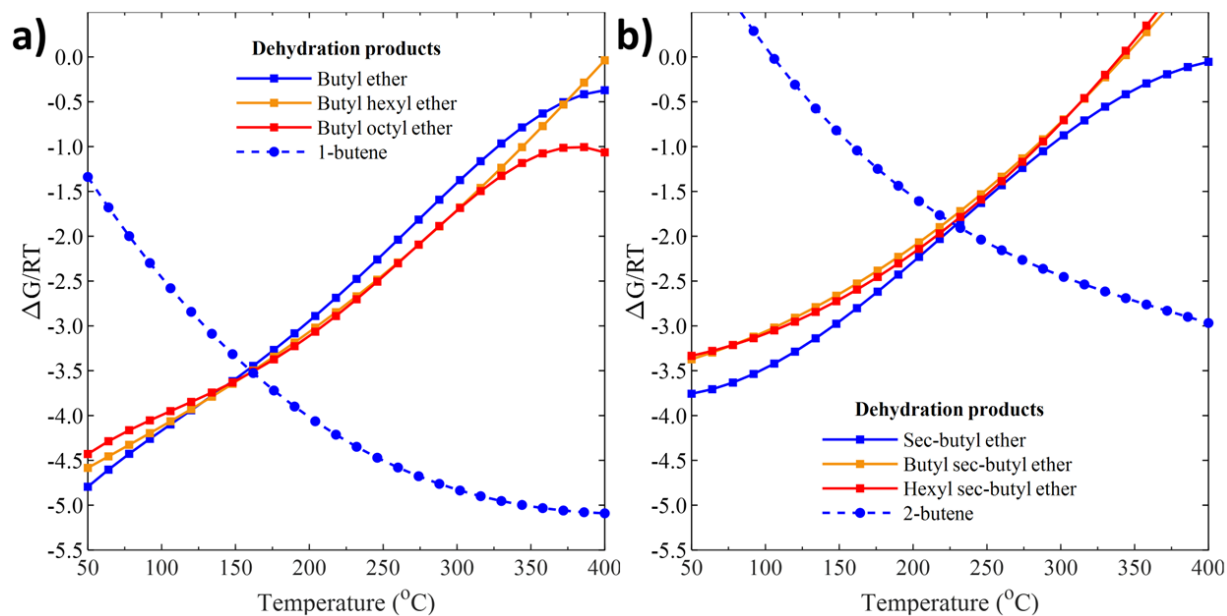


Figure 2. Gibbs free energy of dehydration reactions as a function of temperature. **A)** 1-butanol dehydration reactions and **B)** 2-butanol dehydration reactions. Blue signifies competitive dehydration reactions of the parent alcohol. Conditions: 100 psig.

A thermodynamic analysis of binary alcohols mixtures was analyzed to understand the role of alcohol structure and carbon length on dehydration reactions. Linear, branched, and secondary alcohols were used to compare the Gibbs free energy of the ether products over a wide operating temperature range. In this analysis the ethers have the structure from the parent alcohols. This analysis gives us insight as to the thermodynamically favored dehydration products of different feeds and operating temperatures. In this paper, the operating temperature is 170 °C.

Figure 2 shows the Gibbs free energy as a function of temperature for liquid phase dehydration of 2-butanol and 1-butanol. Thermodynamic data was taken from the NIST database, and the model was implemented using UNIFAC parameters in ASPEN. The reactor pressure was 100 psig, and a temperature range from 50 – 400 °C was modeled. The Gibbs free energy trends were then fit to a polynomial to highlight the trends on the graph.

Figure 2a shows the etherification products for 1-butanol. The free energy formation of ethers of varying linear alcohol feed chain sizes are similar across a wide temperature range, suggesting that bimolecular dehydration is independent of the size of the alcohols in the reaction streams. Both monomolecular and bimolecular dehydration are thermodynamically favorable reactions at temperatures from 50 to 300 °C. As the temperature increases, mono-dehydration becomes more favorable than bimolecular dehydration. The Gibbs free energy is also a function of the alcohol structure. Linear ethers are lower in Gibbs free energy compared to ethers formed from a secondary alcohol.

Figure 2b represents the etherification products of 2-butanol, a secondary alcohol. Monomolecular dehydration of 2-butanol produces 2-butene. Bimolecular dehydration of 2-butanol produces sec-butyl ether. Bimolecular dehydration of 2-butanol with hexanol further produces hexyl-sec butyl ether. At

temperatures below 200 °C, the ethers are the thermodynamically favored product. At higher temperatures olefins are the thermodynamically favored product. However, both monomolecular and bimolecular dehydration are thermodynamically favorable at temperatures from 50 to 300°C. The free energy of formation of hexyl-sec butyl ether and sec butyl ether is similar.

3.2 Dehydration of pure alcohols

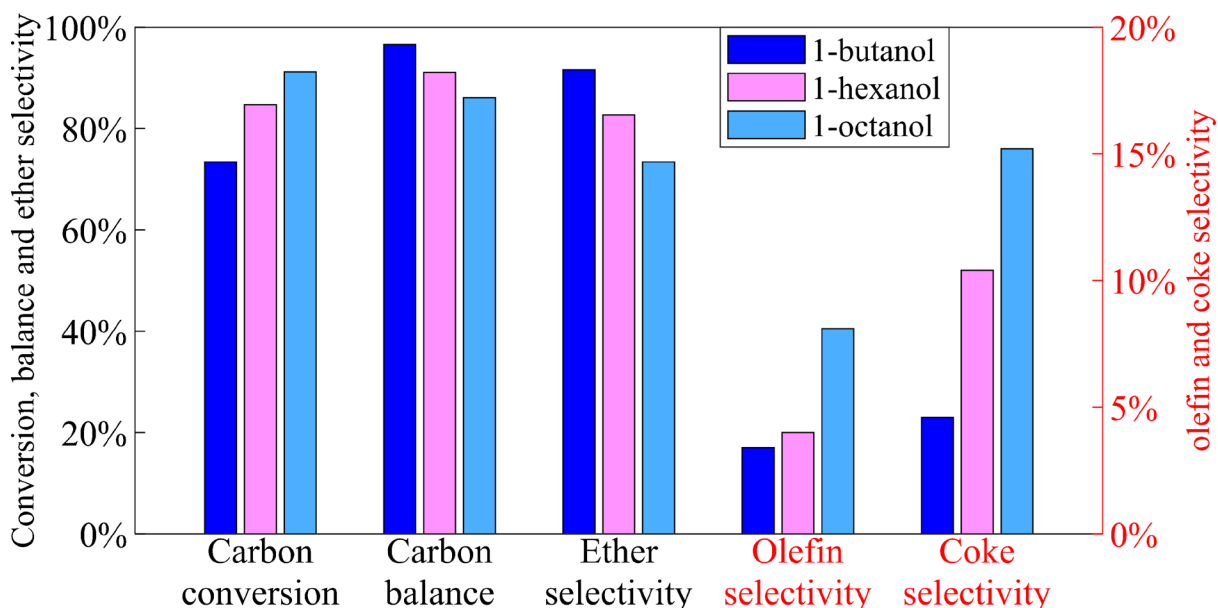


Figure 3. Dehydration of pure alcohol over Zeolite HY. T = 170 °C, P = 100 psig, 0.02 mL/min flowrate, WHSV = 0.54 h⁻¹, TOS > 20 hr.

Linear alcohols were first studied to determine if there are differences in ether selectivity between linear alcohols of varying chain length. It has been reported that mono-dehydration of branched and secondary alcohols have lower activation energies barriers compared to bi-molecular dehydration^{11, 13}. Linear alcohols are the preferred feed to produce bi-molecular dehydration products. Thus varying the chain length could provide insight of any reactivity differences by maintaining the alcohol structure constant.

Figure 3 shows the dehydration reactions of pure alcohol feeds in a continuous flow reactor. All experiments were done at a constant WHSV. The carbon conversion increases with increasing chain length of the alcohol. The carbon balance decreases with increasing alcohol size as the larger alcohols produce more coke (See Tables SI5, SI6 and SI15). The ether selectivity decreases, and the olefin selectivity increases with increasing carbon length of the alcohol. Based on these findings, a C₁₀ alcohol such as 1-decanol would have a coke selectivity around 20%. These results suggest that it would be desirable to remove the C₁₀₊ alcohols from the feed prior to the etherification step. In all pure alcohol feed runs, the catalyst was shown to be stable for over 40 hr TOS, as shown in Figures SI 6 and SI 12.

3.3 The effect of esters in the reaction stream

As shown in Figure 1, the actual products of the alcohol oligomerization reactor also include small concentrations of esters². Depending on the conversion of the oligomerization reactor, the ester concentration can range from less than 2%, to over 10%. Therefore, in this section, the introduction of esters in the dehydration reactor is analyzed to determine if these esters can also be upgraded into diesel-range molecules.

Feedstocks with the code ‘MG’ represent model guerbet alcohol mixtures that assume all esters from the ethanol oligomerization reactor are broken down to their parent alcohols via ester hydrogenolysis. Figure 4 shows the effects of esters on the dehydration step using MG – 12 with different levels of esters. The difference between MG – 12 and SG – 12 is the presence of esters. SG – 12 has an ester content of 1.46 wt%. Another feedstock with 0.15wt% esters is shown in Figure 4 and represents a feedstock with a significant reduction of esters in the reaction stream (see Table SI3). The presence of esters in the reaction stream increases coke selectivity. It has been shown in the literature that esters of varying structure can play a significant role in coking selectivities over acid catalysts¹⁴. As the ester concentration decreases, the ether selectivity and carbon balances increase. Small amounts of esters significantly decrease the carbon balance (See Tables SI7 and SI9).

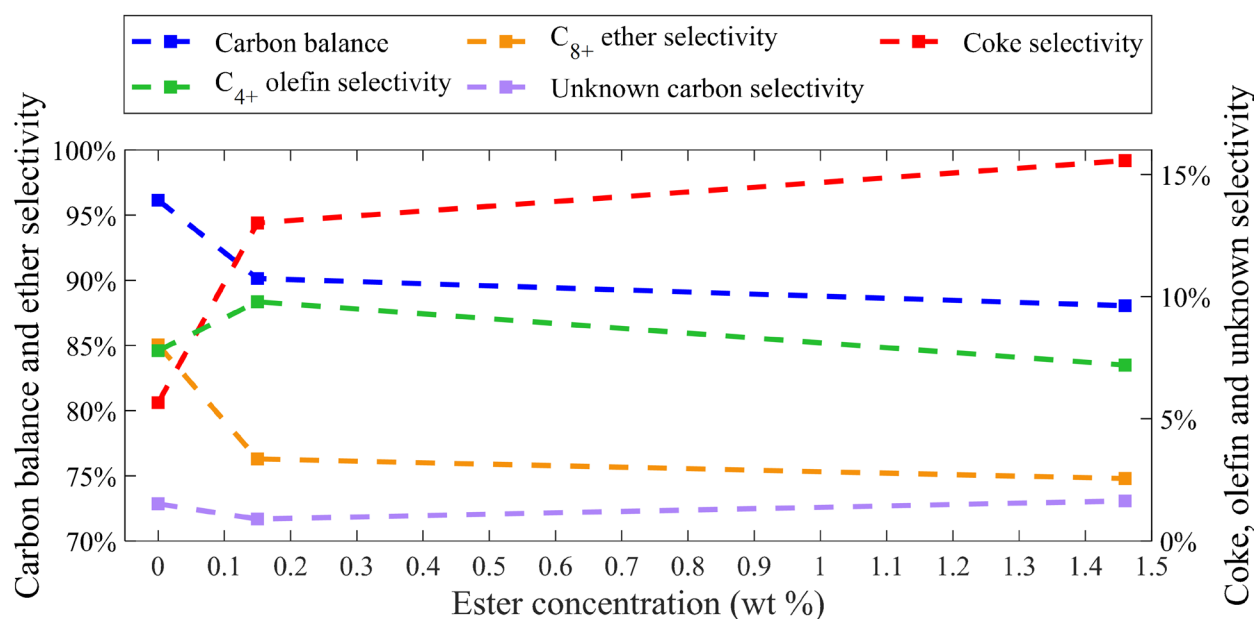


Figure 4. Effect of esters on product selectivity. Feedstock MG – 12 with different levels of esters over zeolite HY. T = 170 °C, P = 100 psig, 0.02 mL/min flowrate, 1.8 g HY, WHSV = 0.54 h⁻¹. Feedstock MG – 12 represents an ideal feedstock with 0 wt% of esters.

As the ester content in the feed increases the heavy oligomer concentration in the product increases. These heavy oligomers are soluble in the alcohol feed. These heavy oligomers have been studied and detected in similar systems, particularly for acid-catalyzed dehydration reactions of sugars from biomass^{15, 16}. Figure SI3 further supports this theory, as the amount of undetected carbon linearly increases with increasing ester concentration. For a more detailed breakdown of coke in the solid and liquid phase, refer to Tables SI8 and SI10.

Therefore, as much of the esters as possible must be removed from the dehydration reactor stream. Ideally, the total alcohol purity of the reactant stream should be above 99.90 wt% to ensure that esters will not significantly change the reaction chemistry (refer to Table S11 and S12 for feedstock comparison with MG – 12 and SG – 12). We conclude that an ester hydrogenolysis step is necessary to produce alcohol rich feedstocks for dehydration. Over zeolites, esters can create side reactions with the reactants and products produced in the dehydration step. Water produced from etherification can catalyze ester hydrolysis reactions. Over zeolites, as the ester is broken down to its respective alcohol and carboxylic acid, both molecules will compete for dehydration sites as shown by Corma and coworkers¹⁷. The adsorption of carboxylic acids is stronger than for alcohols. Thus, the carboxylic acids likely cause a decrease in the number of acid sites that are available for dehydration reactions. Other labs have reportedly seen other adsorption effects over large-pore zeolite catalysts, in which upgrading incoming low-chain esters may be difficult. In the case of benzyl alcohol reacting with acetic acid over H-beta, increasing alcohol concentration led to a decrease in ester selectivity and an increase in ether selectivity¹⁸. This is attributed to alcohols saturating the catalyst surface, blocking acid sites for carboxylic acids to react with other alcohol chains to produce esters.

Esters can be reduced using metals on various supports¹⁹⁻²¹. The esters typically undergo three different reaction pathways which involve 1) C=O bond hydrogenation to produce ethers and water, 2) C-O hydrogenolysis to produce alcohols and aldehydes (and further hydrogenation of the aldehydes to an alcohol) and 3) hydrolysis reactions which produce alcohols, alkenes, and carboxylic acids. In ethanol oligomerization, the esters produced typically fall within the carbon chain length of 8 and under. This makes pathway 1 undesirable, as it would mainly produce C₈ ethers. Pathway 3 is also undesirable as carboxylic acids compete with alcohols for acid sites, decreasing dehydration rates. Pathway 2 is desirable in our applications, as only alcohols and aldehydes are produced. Under an H₂ environment, the remaining aldehydes can be hydrogenated to their respective alcohol, leading to a pure alcohol feedstock that can be fed into the dehydration reactor. As previously mentioned, high ester conversion to alcohols will be necessary to minimize the effects of these molecules in the dehydration stream. As shown by Chavarrio²², high ester conversion into alcohols can be achieved using Cu/ZrO₂ catalysts (~90% conversion). The Cu/ZrO₂ catalyst simultaneously reduces the ester and hydrogenates the corresponding aldehyde. The use of these catalysts were tested with simulated guerbet feedstocks by Restrepo and coworkers²³, in which the ester mol fraction was decreased from 7.6 – 0.3%, resulting in a reduction of ~96% of the ester molar composition. This reduction in ester content led to an increase in the final alcohol mol composition from 92.3 – 99.3%. Thus it is possible to reduce the ester content prior to the dehydration stream using a Cu/ZrO₂ catalyst to produce highly concentrated alcohol streams above 99.96 mol%, or above 99.90 wt%.

3.4 Pressure effects on Dehydration

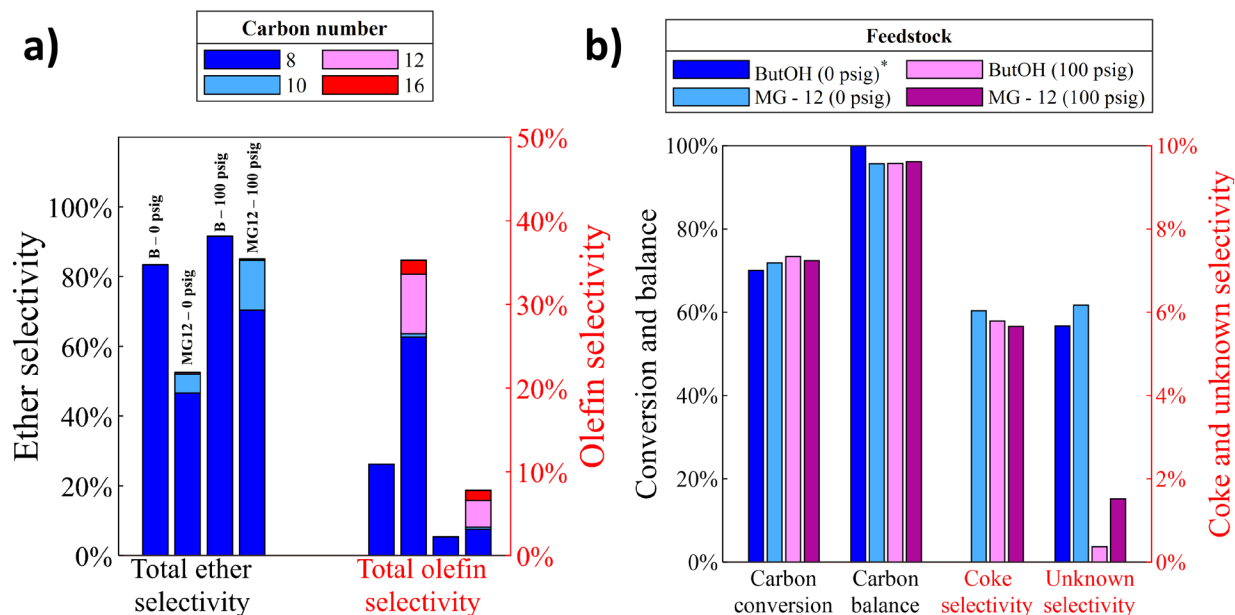


Figure 5. Dehydration distributions of pure 1-butanol and MG-12 feedstock streams. **A)** Final product distributions as a function of carbon number; **B)** Reaction parameters as a function of pressure. $T = 170\text{ }^{\circ}\text{C}$, $P = 0 - 100\text{ psig}$, 0.02 mL/min flowrate, $\text{WHSV} = 0.54\text{ h}^{-1}$, $\text{TOS} > 20\text{ hr}$. For olefins, the numbering is ‘ $n/2$ ’. Values next to feedstock represent operating pressure. Asterisk signifies carbon balances were normalized to 100% due to overestimation of carbon in the liquid phase. ‘B’ signifies a pure n -butanol stream. MG – 12 signifies the model feedstock.

The least complex feedstock, consisting mainly of n -butanol and low amounts of branched and secondary alcohols, was studied as a feed for dehydration to understand the effects of operating pressure. Nel et al reported that changing the operating pressure can affect the ether yields obtained in dehydration reactions²⁴, though a thorough explanation of this phenomenon remains unclear. Furthermore, Nel et al noted these differences with linear alcohols, and not with a mixture of varying alcohol structure content. The effect of pressure was first studied with pure n -butanol. The second feedstock, MG – 12, introduces two different alcohol structures in low concentrations.

The alcohol distribution of MG – 12 is shown in Figure S11, and a detailed breakdown of the feedstock studied can be found in Table S12. The effect of pressure on dehydration was studied with n -butanol and MG – 12 feeds as shown in Figure 5. Figure 5a depicts the carbon number distributions for the ethers and olefins. The left-hand side depicts the selectivities of the ethers based on carbon number, while the right-hand side depicts the selectivities of the olefins based on carbon number. In all cases, the olefin selectivity was lower than the ether selectivity. Figure 5b depicts that increasing the pressure does not affect the conversion or carbon balances with the butanol and MG – 12 feeds. In all cases, the unknown products were below 10% selectivity. For pure n -butanol, pressure had minimal impact on the product distributions. The ether selectivity slightly increases, and the olefin selectivity slightly decreases with pressure for n -butanol, (Figure 5a). For n -butanol at 0 psig, the true coke selectivity based on TOC experiments is 3.5% (see Table S18). In Figure 5b, the coke selectivity is zero as the carbon balances were over 100% when only the gas and liquid phase were analyzed. This is because the final mass balances obtained from the HPLC pump were over 100% when only gas and liquid products were considered. A noticeable pressure effect is observed with MG – 12 (See Tables S17 and S18). One plausible explanation is that pressurizing the system

above the reactant vapor pressures shifts the reaction phase from gas to liquid (See table SI11). Due to the significant change in selectivities, all further reactions were conducted at 100 psig.

3.5 Dehydration of Model feedstocks

As previously shown increasing the chain length of the linear alcohols resulted in higher coke and olefin selectivities. In this section, the complex mixtures obtained from the ethanol oligomerization reactor vary based on alcohol structure and chain length. These mixtures will create a pool of ethers, where the final products produced will be determined based on the alcohol structure and size of all alcohols introduced in the dehydration reactor. Therefore, the final size of the ethers produced from the dehydration reactor will be highly dependent on the incoming size and structural content of the alcohol feedstocks.

Rorrer and Eagan reported that alcohol structure is important in etherification, in which high linear alcohol streams increase the rate of etherification^{11, 13}. However, the feeds they used were single alcohol feeds, linear alcohol-only mixtures, or binary reaction mixtures of linear and branched alcohols. While branched alcohols can still undergo etherification to some extent, secondary alcohols will mainly produce olefins. It is therefore unclear how complex C₄₊ alcohol distributions affect the final size and selectivities for ether and olefin distributions obtained from competitive dehydration reactions. Other groups have studied etherification of alcohols over polymeric acidic resin catalysts (i.e Amberlyst 70), though these catalysts typically suffer from swelling due to water being formed during dehydration reactions, and thus catalyst stability further becomes an issue at temperatures above 150 °C^{11, 25-28}. H-exchanged zeolites are robust catalysts that are not affected by swelling, though dealumination may be important in high water content streams and/or at reaction temperatures above 170 °C^{29, 30}. The recent advancements in understanding the effects of water on zeolite structure suggest that these materials will be of interest for future processes that require water-tolerant catalysts for dehydration reactions³¹.

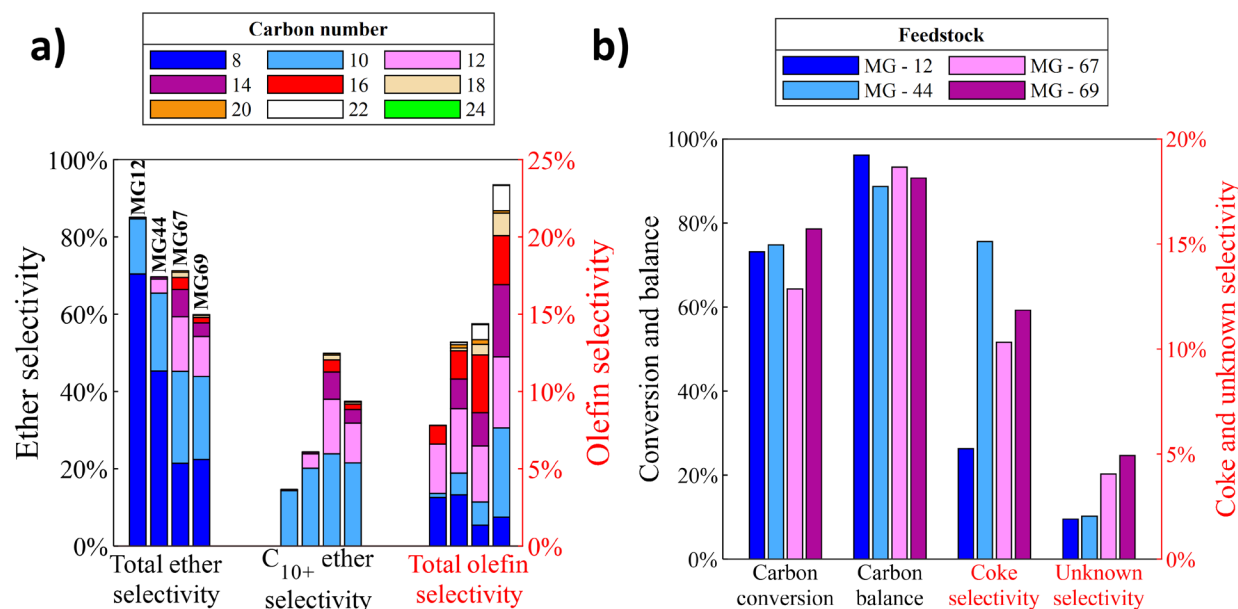


Figure 6. Dehydration distributions of model feedstocks. **A)** Final product distributions as a function of carbon number and structure; **B)** Reaction parameter distributions as a function of ethanol conversion. $T = 170\text{ }^{\circ}\text{C}$, $P = 100\text{ psig}$, 0.02 mL/min flowrate, $\text{WHSV} = 0.54 - 0.61\text{ h}^{-1}$, $\text{TOS} > 30\text{ hr}$. For olefins, the numbering is ‘n/2’. Colors not visibly shown for compounds are present in low amounts ($< 1.0\%$). ‘MG’ followed by the value represents the model feedstock obtained at the respective ethanol conversion in the ethanol oligomerization step.

Figure 1 depicts the molecular distribution of four different feedstocks obtained from an ethanol oligomerization reactor¹. As the ethanol conversion increases, larger fractions of branched and secondary molecules are present in the reaction stream. The ester composition further increases with increasing ethanol conversion. As shown in Scheme 1, all the esters are assumed to undergo 100% hydrogenolysis conversion to produce alcohol-rich streams. The alcohol-rich feedstocks are then used for the dehydration step to produce diesel-range ethers and olefin fuel precursors. These alcohol-rich streams are depicted in Figure SI2, and a detailed breakdown can be found in Table SI2. Some alcohols were substituted for a commercially available alcohol because those alcohols could not be purchased commercially. For example, 2-ethyl-1-hexanol (C_8) was used in place of C_{10+} branched alcohols (2-ethyl-1-octanol, 2-ethyl-1-decanol, and 2-ethyl-1-dodecanol). For secondary alcohols, C_{15+} secondary alcohols (were 4-undecanol, 4-tridecanol, 2-pentadecanol, and 2-heptadecanol) were replaced with 2-undecanol (C_{11}). The lumping method was used to maintain the structural composition of linear, branched, and secondary alcohols.

Figure 6 is the product selectivity, conversion and carbon balance obtained from the four model feedstocks studied with Table SI12 and SI13 showing more details. Figure 6a shows that as the linear alcohol content of the feed decreases the C_{8+} ether selectivity decreases. The olefin selectivity increases as the branched and secondary alcohol content of the feed increases. As shown by the C_{10+} ether selectivities, feedstocks with larger fractions of C_{6+} alcohols shift the ether selectivity from C_{8+} to C_{10+} ethers. The increase in C_{6+} alcohol content also shifts the olefin selectivity from C_{4+} to C_{6+} olefins. The unknown carbon detected increases with increasing complexity of the feedstock. Figure 6b shows that the carbon balance decreases with increasing ethanol conversion. This effect is likely due to an increase in the C_{6+} alcohol content, branched alcohols, and secondary alcohols of the feed.

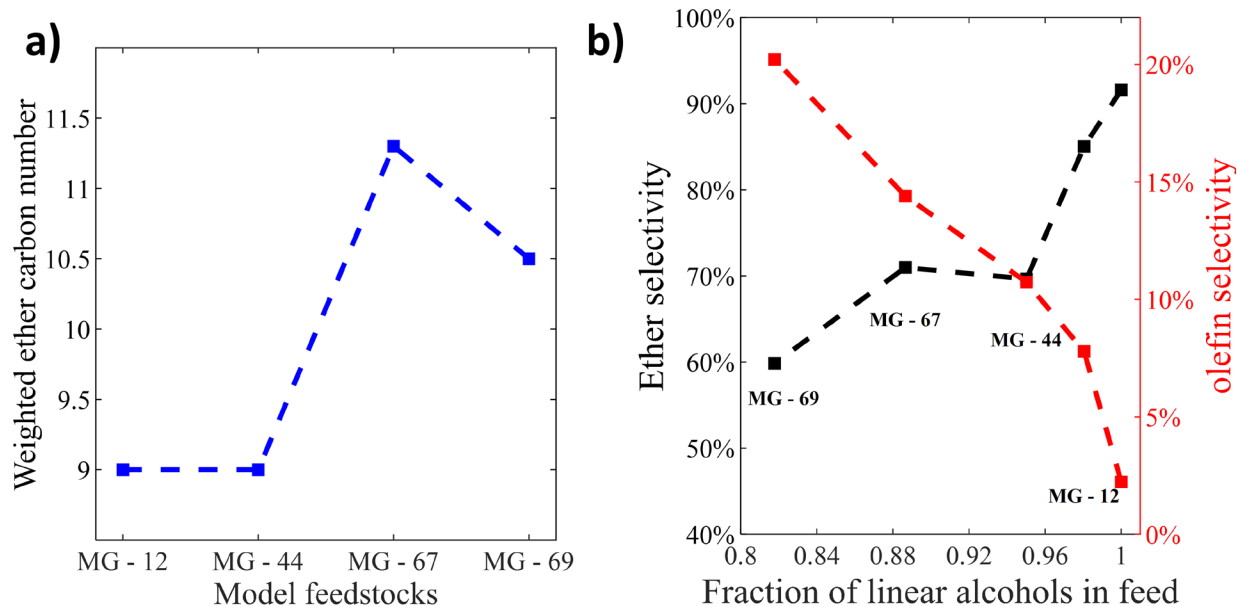


Figure 7. **A)** Average carbon number of ethers produced as a function of ethanol conversion. Product carbon numbers were calculated based on total ether product analyzed in the liquid phase and **B)** Product selectivities of model feedstocks as a function of linear alcohol content. $F = 1$ represents a pure 1-butanol stream as a reference reaction.

Both MG-67 and MG-69 have similar branched alcohol content (7.4 mol% vs. 6.9 mol%, respectively). However, the secondary alcohol content is 7 mol% higher for MG-69. The increase in secondary alcohol content led to an increase in coke selectivity on the catalyst surface by about 4% (See Table SI13). While larger chain alcohols are present in MG-69, the linear alcohol distribution is similar (see Table SI2, L/B and L/S ratios). Thus, secondary alcohols can lead to higher surface coke selectivities. While branched alcohols can still undergo bi-molecular dehydration to some extent, secondary alcohols are less likely to produce ethers and mainly undergo mono-dehydration. Secondary alcohols may either be adsorbing strongly over HY, or the olefins produced are possibly undergoing side reactions (i.e. acid-catalyzed oligomerization), leading to a decrease in the carbon balance via coking mechanisms^{32, 33}. The olefins produced from branched alcohols can also undergo the same side reactions that secondary alcohol derived olefins encounter, though reactivity differences to coke products are still unclear. We conclude that secondary alcohols will likely not undergo etherification at our current conditions, with olefins the main by-products from secondary alcohols. The increase in secondary alcohol content led to an increase in the overall coke selectivity by about 1.5%. Further increasing the secondary alcohol content will lead to higher coke selectivities (See Table SI12). The increase in secondary alcohol content can lower the final blend stock yields, as well as increase the CO₂ emissions produced from coke removal through catalyst regeneration. Measuring the amount of carbon on the catalyst after reaction was done using total organic carbon content (TOC) analysis (see Table SI16). The catalyst bed of MG-67 had a higher coke content than MG-69.

As shown in Figure 7a the size of the ethers does not increase from feedstock MG-12 to MG-44 likely because the n-butanol content in both feedstocks was similar (91.8 vs. 82.20 mol %, respectively). However, the ether size increases from 9.0 to 11.3 with feedstock MG-67. MG-67 has lower n-butanol content (67.88 mol %), while also having higher fractions C₆₊ linear and branched alcohols. The ether size decrease to 10.5 with feedstock MG-69 likely due to the higher fractions of secondary alcohols. Figure 7b shows the ether and olefin selectivities as a function of the alcohol linearity of the feedstock. The ether selectivity decreases with decreasing linear alcohol fraction in the feed. This trend is consistent with other

studies^{11, 13}. As the fraction of linear alcohols continues to decrease, coking and mono-dehydration reactions become more prominent. We conclude that high linear alcohol streams above 80 mol% are needed to maintain the C₈₊ ether selectivity above 60%.

3.6 Dehydration of oligomerization feeds from ethanol and n-butanol mixtures

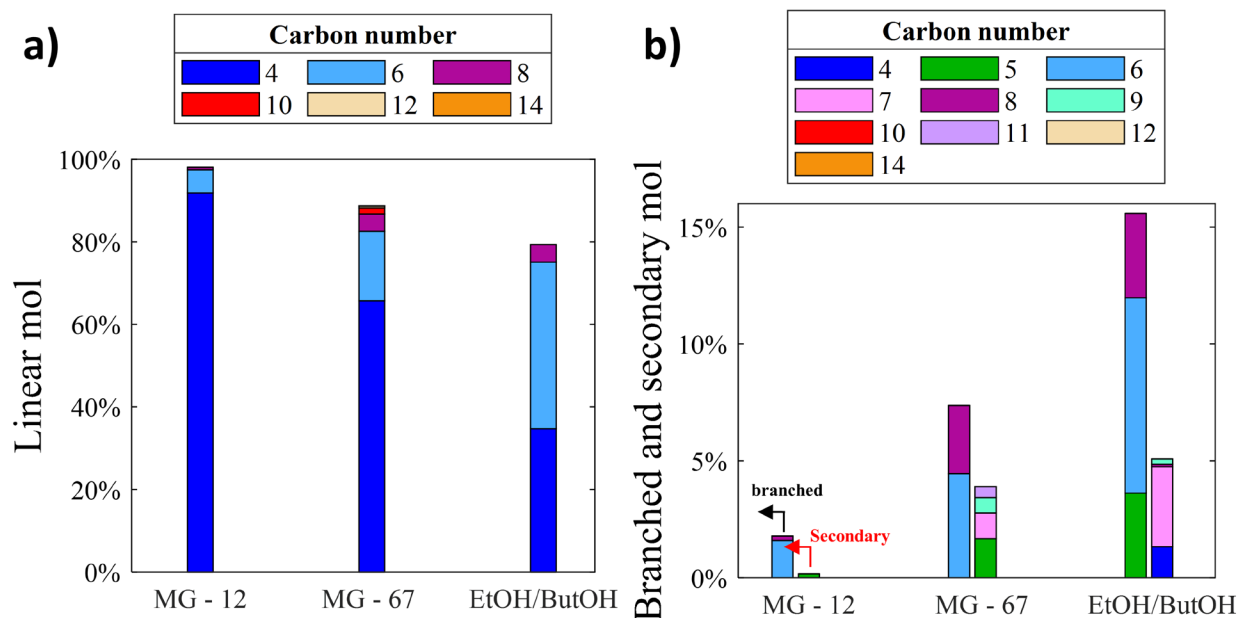


Figure 8. Alcohol distribution from Guerbet conversion of ethanol with EtOH/ButOH oligomerization products. **A)** represents the linear alcohol distribution and **B)** represents the branched and secondary alcohol distributions. Secondary alcohol numbering is defined by ‘n’. Colors not visibly shown for compounds are present in low amounts (< 1.0%).

Both the alcohol structure and size play a role in the final ether distributions as shown in Figure 7. Increasing the branched and secondary alcohol concentration, as well as the alcohol size, leads to a decrease in the total ether selectivity. At the same time, there was an increase in the C₁₀₊ ether selectivity. The C₁₀₊ ether selectivity decrease once there was a significant fraction of secondary alcohols in the feedstock. Therefore, heavy alcohol feedstocks with low secondary alcohol concentrations will be the ideal mixtures to shift the ether yields from the C₈ to C₁₀₊ range, as these ethers are the ideal candidates for drop-in diesel fuel. Tuning the incoming alcohol feedstock to higher carbon numbers can lead to an increase in the diesel #2 yield, as fuel yield is an important economic factor in the ethanol to diesel process².

Our research team has shown that the C₁₀₊ ethers can be maximized by feeding in a mixture of ethanol and butanol into the Guerbet reactor²³. Figure 8 shows the products from the Guerbet reaction for MG – 12, MG – 67 and ethanol/butanol (EtOH/ButOH) oligomerization. These feeds were then used for the dehydration reaction. A detailed breakdown of the EtOH/ButOH oligomerization feedstock can be found in Table SI4. MG – 12 was chosen as it has the lowest selectivity to C₁₀₊ ethers, while MG – 67 was chosen as it has the highest selectivity to C₁₀₊ ethers. The EtOH/ButOH oligomerization step assumes that un-reacted n-butanol from the process can be separated and recycled back into the ethanol oligomerization step. Recycling of n-butanol increases the overall C₆₊ alcohol content from the Guerbet feed. However, the linear alcohol content decreases when the butanol is recycled. The increase in branched alcohol content is expected due to the addition of n-butanol to the oligomerization step, as nucleophilic alcohols that are larger than ethanol react to form larger branched products^{11, 34}. The secondary alcohol content slightly increases

with butanol addition compared to MG – 67. The alcohols from the feeds in Figure 8 were then used for dehydration. Table SI13 and SI14 show the detailed dehydration products from MG – 12, MG – 67 and the EtOH/ButOH oligomerization products. The carbon balances are lower for the EtOH/ButOH products at $\text{WHSV} = 0.54 \text{ h}^{-1}$, as well as the overall ether selectivity. The WHSV was doubled to assess the effects on carbon balance. Table SI14 shows that doubling the space velocity has a negligible effect on the carbon balances and slightly increasing the C_{10+} ether selectivity. While higher WHSVs lead to higher selectivities, the conversion further decreases. Here, determining the quality of the raw blends produced from an economic point of view should be assessed by engine testing. The supported engine testing can then help provide a sensitivity analysis on whether the slight increases in carbon balances produce better raw blends, while minimizing the amount of recycled reactant materials. This kind of analysis has been shown by Restrepo-Florez and coworkers², where surrogate blends were tested, and the information was feed into a techno-economic analysis to understand the economic factors of the ethanol to diesel route.

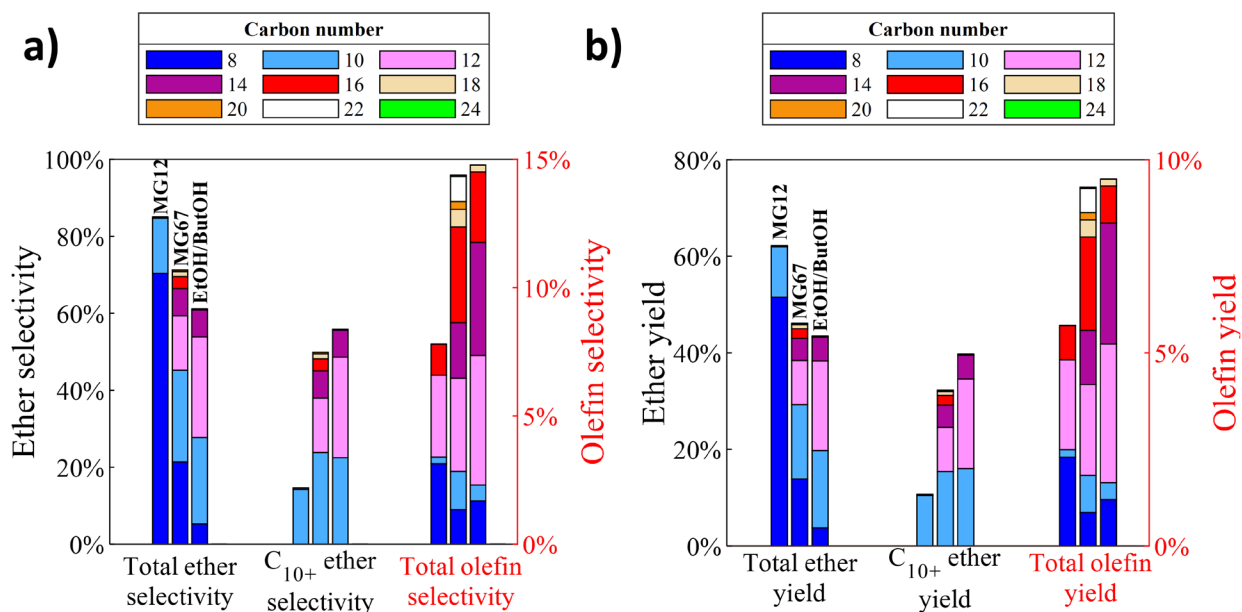


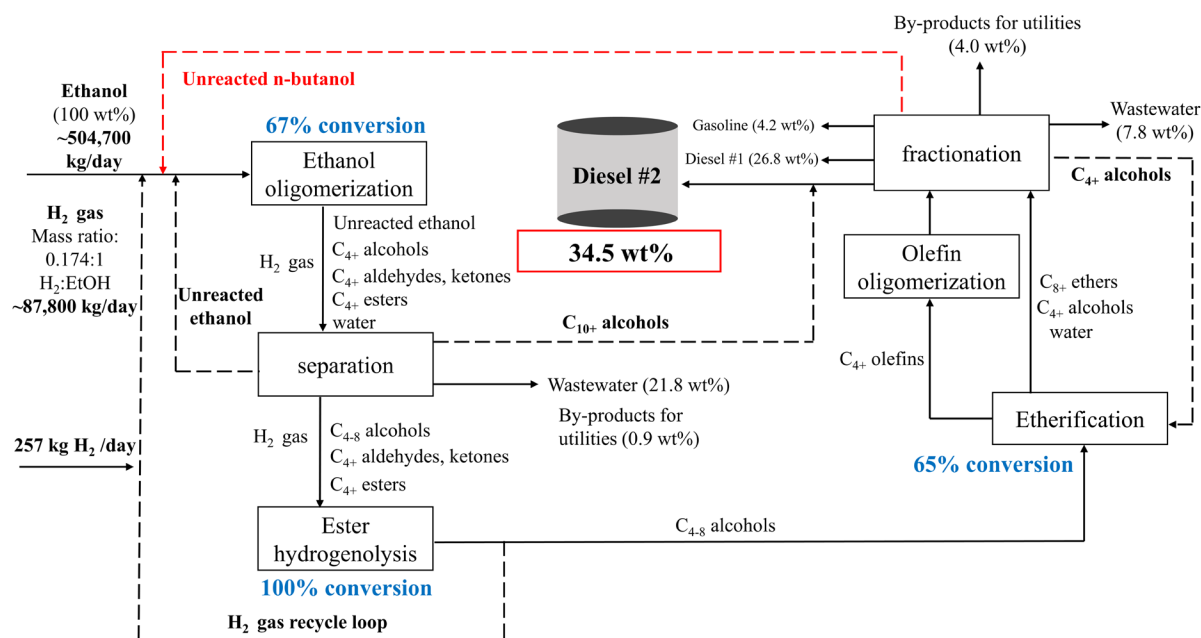
Figure 9. **A)** Selectivity distributions of ethers and olefins and **B)** Yield distributions of ethers and olefins. For MG – 12 and MG 67, the $\text{WHSV} = 0.54 \text{ h}^{-1}$ (Flowrate = 0.02 mL/min) with TOS > 30 hr. For the EtOH/ButOH oligomerization products, the $\text{WHSV} = 1.0 \text{ h}^{-1}$ (Flowrate = 0.04 mL/min) with TOS ~ 21 hr. $T = 170 \text{ }^\circ\text{C}$, $P = 100 \text{ psig}$. For olefins, the numbering is defined as ‘n/2’.

As shown in Figure 9a, the C_{10+} ether selectivity obtained from MG-67 is 50%, while the C_{10+} ether selectivity is 56% using the EtOH/ButOH product stream. As shown with the linear alcohol feeds, larger alcohols can lead to lower carbon balances and lower overall ether selectivity. This may explain why the selectivity only increased by less than 10% across the two feedstocks. Figure 9b shows the ether and olefin yields. The C_{10+} ether yield increases because of the presence of larger fractions of C_{6+} alcohols for MG – 12 and MG – 67 (11% vs 32%). The EtOH/ButOH oligomerization products further support that while stronger alcohol adsorption effects may be present, larger fractions of C_{6+} alcohols increase the C_{10+} ether yield. The C_{10+} ether yield for MG – 67 was 32%, while for the dehydration of EtOH/ButOH oligomerization products the C_{10+} ether yield was 40%. Furthermore, the butyl ether yield was lower for the dehydration of EtOH/ButOH oligomerization products compared to MG – 67 (4% vs. 14%). The implementation of an n-butanol recycling unit can therefore be used to significantly reduce the production of C_8 ethers and shift the final product carbon number to the C_{10+} range. Because EtOH/ButOH

oligomerization products were used to represent a recycle feed stream of n-butanol, it is therefore possible to further increase the C₁₀₊ ether yields while re-using unconverted alcohol in the dehydration steps.

The coke content on the catalyst was measured after using the MG – 12, MG – 67 and EtOH/ButOH feeds. The graphs for these experiments can be found in Figure SI4. In all cases, the presence of both soft coke and hard coke is observed on all beds. Volatile compounds are within the temperature region of 50 – 200 °C. The soft coke region is in the temperature range of 200 – 400 °C, while the hard coke region is in the temperature range of 400 – 600 °C³⁵. In all cases when oxygen is present, the largest change in weight occurs within the volatile and soft coke region. In the nitrogen experiments, there is minimal change in weight between the region of 400 – 600 °C. In all cases, the lowest mass change is in the hard coke region. This trend is also observed when analyzing the EtOH/ButOH oligomerization beds, in which most of the weight loss is in the volatile compound region.

3.7 Overall process of the ethanol to diesel route



Scheme 2. Proposed process diagram of ethanol to diesel fuel range ethers. Important design parameters are represented by dashed lines. Red line signifies the proposed n-butanol recycling unit and is not considered in the final mass balance. Fuel yields and mass outputs are shown on a dry ethanol basis. The hydrogen balance is based on an ethanol oligomerization reactor operating at 325 °C and 300 psig, with a partial pressure ratio of 4:1 for H₂: Ethanol. Most of the hydrogen is recycled, therefore low amounts of hydrogen is further added into the system. The daily bio-ethanol production is based on the production of approximately 60 MMgal/year of anhydrous ethanol. Data and overall process diagram is derived from².

Scheme 2 represents a block-flow diagram of the proposed ethanol to diesel technology. In the first step, ethanol is oligomerized at around 67% single pass-conversion to produce the reactant oxygenate distribution. Water removal will be needed throughout the process, as it is known to inhibit etherification reactions^{11, 36, 37}. In the second step ester hydrogenolysis, the esters undergo hydrogenolysis to their parent alcohols and ketones. Aldehydes and acetals are hydrogenated to their respective alcohols in this same step. C₁₀₊ alcohols are then removed and blended directly into diesel. These C₁₀₊ alcohols have properties suitable

for diesel #2. Water is also removed prior to dehydration. The alcohol rich feedstocks are then used as a feed for the dehydration reactor at 65% single pass carbon conversion. The final product is then further separated, and the raw blend is cut into three specific fuel grades. Lighter alcohols are distilled and sent back to the oligomerization reactor. The final diesel #2 yield obtained with this approach is 34.5 wt% or 49.5 carbon % on a dry ethanol basis². The composition of the final diesel #2 blend can be found in Table SI31 in SI Section 6. The byproducts of this process include hydrogen and light gases (i.e olefins and paraffins) used for utilities (i.e steam generation), as well as wastewater produced from ethanol oligomerization and dehydration. Diesel #1 is mainly composed of di-butyl ether, while the gasoline fraction mainly consists of light molecules such as C₁ – C₂ alcohols, esters and olefins. The addition of a n-butanol recycling unit would further increase the alcohol size of the incoming dehydration feedstock. The increase in feedstock size allows us to further increase the chain sizes of the final ethers produced in the blend. A rigorous process analysis of this process is reported by Restrepo – Florez and coworkers²³.

Our approach to produce diesel range products outlined in this paper is the highest yield diesel fuel from ethanol technology reported in the literature. Several other approaches produce gasoline range products or jet fuel mixed with gasoline. For example a single stage ethanol to jet, using a zeolite catalyst, produces around 40 – 70 C% aromatics³. In this approach 30 - 60 C% may be used for distillate fuel applications, and the mixture may only be blended in low amounts unless the aromatics are distilled³. A two-stage ethanol to jet fuel process, the maximum fuel yield can be around 65 – 70 C%³.

4 Conclusions

Alcohols can be dehydrated into ethers using zeolite-based catalysts in a continuous flow reactor. Olefins and coke are the undesired reactions. Mono- and Bi-molecular dehydration reactions for linear alcohols are thermodynamically favorable at the temperature (170 °C) used in this study. Secondary alcohols prefer mono-molecular dehydration at the reaction conditions used in this study. Bi-molecular dehydration is thermodynamically more favorable than mono-molecular dehydration at temperatures less than 190°C for linear alcohols. Esters can cause undesired coke formation in the dehydration step. Dehydration experiments concluded that increasing the pressure from gas to liquid increases ether selectivity. Experiments showed that the pressurized reactions are stable for up to 50 hr TOS, and evidence of deactivation is present with esters at 1.5 wt% before 50 hours. Branched alcohol and secondary alcohols are more selective to olefins, while linear alcohols promote cross-etherification of branched alcohols. Feedstocks with high linear alcohol content led to higher ether selectivities. Feedstocks with higher branched and secondary alcohol content are more likely to produce a distribution of C₄₊ olefins. Increasing the secondary alcohol content was shown to increase coke selectivities. It was shown that for pure linear alcohol feeds, the ether selectivity decreases as a function of carbon chain length. However, feedstocks with larger fractions of C₆₊ alcohols were shown to be more selective towards C₁₀₊ ethers. Small chain olefins can be oligomerized and hydrogenated to distillate range paraffins, while the ethers produced can be directly blended into diesel. As C₁₀₊ ethers are better candidates for diesel #2, understanding the trade-off between alcohol chain length and C₁₀₊ ether yields will be crucial to produce biodiesel blends capable of being used in freight fuels. Without n-butanol recycling a 34.5 wt% (49.5 carbon %) yield of diesel #2 can be achieved from ethanol. The diesel #2 yield can further increase by recycling of n-butanol.

Author contributions

Emmanuel Canales: conceptualization, data curation, formal analysis, investigation, methodology, software, visualization, writing – original draft. Samuel C. Hower: conceptualization, data curation, formal analysis, investigation, methodology. Daniel Paul Li: data curation, investigation. Aditya Tambe: data curation, formal analysis, investigation. George W. Huber: conceptualization, methodology, resources,

funding acquisition, supervision, project administration, writing – review & editing. David A. Rothamer: conceptualization, resources, funding acquisition, supervision, project administration, writing – review & editing.

Conflicts of interest

There are no conflicts to declare.

Acknowledgements

We would like to thank Dustin Witkowski for providing the flashpoint temperature data for alcohols and ethers in this article. We would also like to thank Juan-Manuel Restrepo-Florez for providing the detailed composition of the Diesel #2 blend.

This work was supported and financed by the U.S. Department of Energy – Vehicle Technology Office (DOE-VTO), based upon work supported by the U.S. Department of Energy's Office of Energy Efficiency and Renewable Energy (EERE) under the Bioenergy Technologies Office, Cooptimization of Fuels and Engines (Co-optima) initiative award number DE-EE0008480. The views expressed in this manuscript do not necessarily represent the views of the U.S. Department of Energy or the United States Government.

References

1. P. A. Cuello-Penalzoa, R. G. Dastidar, S.-C. Wang, Y. Du, M. P. Lanci, B. Wooller, C. E. Kliewer, I. Hermans, J. A. Dumesic and G. W. Huber, *Applied Catalysis B: Environmental*, 2022, **304**, 120984.
2. J.-M. Restrepo-Flórez, P. Cuello-Penalzoa, E. Canales, D. Witkowski, D. A. Rothamer, G. W. Huber and C. T. Maravelias, *Sustainable Energy & Fuels*, 2023, **7**, 693-707.
3. N. M. Eagan, M. D. Kumbhalkar, J. S. Buchanan, J. A. Dumesic and G. W. Huber, *Nature Reviews Chemistry*, 2019, **3**, 223-249.
4. R. A. Dagle, A. D. Winkelman, K. K. Ramasamy, V. Lebarbier Dagle and R. S. Weber, *Industrial & Engineering Chemistry Research*, 2020, **59**, 4843-4853.
5. *Alternative Fuels Data Center*, https://afdc.energy.gov/fuels/ethanol_benefits.html, (accessed January 10 2023).
6. *2018 Outlook for Energy: A View to 2040*, ExxonMobil, Irving, 2018.
7. J. C. González Palencia, V. T. Nguyen, M. Araki and S. Shiga, *Energies*, 2020, **13**, 2459.
8. D. Smith, R. Graves, B. Ozpineci, P. Jones, J. Lustbader, K. Kelly, K. Walkowicz, A. Birky, G. Payne and C. Sigler, *An Assessment of Technology and Knowledge Gaps (US DOE report ORNL/SPR-2020/7)*, 2019.
9. J. Heveling, A. van der Beek and M. de Pender, *Applied catalysis*, 1988, **42**, 325-336.
10. P. A. Cuello-Penalzoa, J. Chavarrio-Cañas, Y. Du, M. P. Lanci, D. A. Maedke, J. A. Dumesic and G. W. Huber, *Applied Catalysis B: Environmental*, 2022, **318**, 121821.
11. N. M. Eagan, B. M. Moore, D. J. McClelland, A. M. Wittrig, E. Canales, M. P. Lanci and G. W. Huber, *Green Chemistry*, 2019, **21**, 3300-3318.
12. N. A. Huq, X. Huo, G. R. Hafenstine, S. M. Tiffit, J. Stunkel, E. D. Christensen, G. M. Fioroni, L. Fouts, R. L. McCormick and P. A. Cherry, *Proceedings of the National Academy of Sciences*, 2019, **116**, 26421-26430.
13. J. Rorrer, S. Pindi, F. D. Toste and A. T. Bell, *ChemSusChem*, 2018, **11**, 3104-3111.
14. M. Bertero, G. de la Puente and U. Sedran, *Renewable Energy*, 2013, **60**, 349-354.
15. I. Van Zandvoort, Y. Wang, C. B. Rasrendra, E. R. van Eck, P. C. Bruijninx, H. J. Heeres and B. M. Weckhuysen, *ChemSusChem*, 2013, **6**, 1745-1758.

16. I. Van Zandvoort, E. J. Koers, M. Weingarth, P. C. Bruijnincx, M. Baldus and B. M. Weckhuysen, *Green Chemistry*, 2015, **17**, 4383-4392.
17. A. Corma, H. Garcia, S. Iborra and J. Primo, *Journal of Catalysis*, 1989, **120**, 78-87.
18. S. R. Kirumakki, N. Nagaraju and S. Narayanan, *Applied Catalysis A: General*, 2004, **273**, 1-9.
19. C. E. Berdugo-Díaz, Y. S. Yun, M. T. Manetsch, J. Luo, D. G. Barton, X. Chen and D. W. Flaherty, *ACS Catalysis*, 2022, **12**, 9717-9734.
20. Y. S. Yun, C. E. Berdugo-Díaz, J. Luo, D. G. Barton, I. Chen, J. Lee and D. W. Flaherty, *Journal of Catalysis*, 2022, **411**, 212-225.
21. J. Schittkowski, K. Tölle, S. Anke, S. Stürmer and M. Muhler, *Journal of catalysis*, 2017, **352**, 120-129.
22. Javier E. Chavarrio, Kyle Kirkendall-Jones and George W. Huber, Submitted to *ACS catalysis*, 2024.
23. J.-M. Restrepo-Flórez, J. E. Chavarrio, E. Canales, P. Cuello-Peñaloza, D. Witkowski, S. Subramanian, D. A. Rothamer and C. T. M. G. W. Huber, *Energy and Environmental Science*, submitted.
24. R. J. Nel and A. de Klerk, *Industrial & engineering chemistry research*, 2009, **48**, 5230-5238.
25. J. H. Badia, C. Fité, R. Bringué, E. Ramírez and M. Iborra, *Journal of industrial and engineering chemistry*, 2016, **42**, 36-45.
26. J. Guilera, E. Ramírez, C. Fité, M. Iborra and J. Tejero, *Applied Catalysis A: General*, 2013, **467**, 301-309.
27. J. Tejero, F. Cunill, M. Iborra, J. Izquierdo and C. Fité, *Journal of molecular catalysis A: chemical*, 2002, **182**, 541-554.
28. R. Bringué, M. Iborra, J. Tejero, J. F. Izquierdo, F. Cunill, C. Fité and V. J. Cruz, *Journal of Catalysis*, 2006, **244**, 33-42.
29. W. Lutz, H. Toufar, R. Kurzhals and M. Suckow, *Adsorption*, 2005, **11**, 405-413.
30. R. Dimitrijevic, W. Lutz and A. Ritzmann, *Journal of Physics and Chemistry of Solids*, 2006, **67**, 1741-1748.
31. R. Simancas, A. Chokkalingam, S. P. Elangovan, Z. Liu, T. Sano, K. Iyoki, T. Wakihara and T. Okubo, *Chemical Science*, 2021, **12**, 7677-7695.
32. M. Guisnet and P. Magnoux, *Applied Catalysis A: General*, 2001, **212**, 83-96.
33. C. H. Bartholomew, *Applied Catalysis A: General*, 2001, **212**, 17-60.
34. N. M. Eagan, M. P. Lanci and G. W. Huber, *ACS Catalysis*, 2020, **10**, 2978-2989.
35. R. Ahmed, C. Sinnathamb and D. Subbarao, *Journal of Applied Sciences*, 2011, **11**, 1225-1230.
36. I. Hoek, T. Nijhuis, A. Stankiewicz and J. Moulijn, *Applied Catalysis A: General*, 2004, **266**, 109-116.
37. M. Kang, J. F. DeWilde and A. Bhan, *ACS catalysis*, 2015, **5**, 602-612.